

Mixed Hierarchy Network for Image Restoration

Hu Gao, Depeng Dang

Abstract—Image restoration is a long-standing low-level vision problem, e.g., deblurring and deraining. In the process of image restoration, it is necessary to consider not only the spatial details and contextual information of restoration to ensure the quality but also the system complexity. Although many methods have been able to guarantee the quality of image restoration, the system complexity of the state-of-the-art (SOTA) methods is increasing as well. Motivated by this, we present a mixed hierarchy network that can balance these competing goals. Our main proposal is a mixed hierarchy architecture, that progressively recovers contextual information and spatial details from degraded images while we use simple blocks to reduce system complexity. Specifically, our model first learns the contextual information at the lower hierarchy using encoder-decoder architectures, and then at the higher hierarchy operates on full-resolution to retain spatial detail information. Incorporating information exchange between different hierarchies is a crucial aspect of our mixed hierarchy architecture. To achieve this, we design an adaptive feature fusion mechanism that selectively aggregates spatially-precise details and rich contextual information. In addition, we propose a selective multi-head attention mechanism with linear time complexity as the middle block of the encoder-decoder to adaptively retain the most crucial attention scores. What's more, we use the nonlinear activation free block as our base block to reduce the system complexity. The resulting tightly interlinked hierarchy architecture, named as MHNet, delivers strong performance gains on several image restoration tasks, including image deraining, and deblurring.

Index Terms—Image restoration, deblurring, deraining, global information, mixed hierarchy architecture.

I. INTRODUCTION

IMAGE restoration, such as image deblurring and image deraining is a family of inverse problems for obtaining a high-quality image from a corrupted input image. The image restoration is generally modeled as follows:

$$l(x, y) = h(x, y) \cdot g(x, y) + \sigma(x, y) \quad (1)$$

Where $l(x, y)$, $h(x, y)$ denote an observed low-quality image, and its corresponding high-quality image, respectively. And $g(x, y)$, $\sigma(x, y)$ denote the degradation function and the noise during the imaging and transmission processes, respectively. Image restoration aims to enhance the visual quality of images $l(x, y)$ and get the high-quality image $h(x, y)$. It is typically an ill-posed inverse problem since there are many candidates for any original input and the image degradation procedures are irreversible. To restrict the infinite feasible solutions space to natural images, traditional methods [1]–[5] explicitly design domain-relevant priors, task-relevant priors, and various constraints for the given kind of restoration

Hu Gao and Depeng Dang are with the School of Artificial Intelligence, Beijing Normal University, Beijing 100000, China (e-mail: gao_h@mail.bnu.edu.cn, ddepeng@bnu.edu.cn).

problem. Then, with the appropriately designed priors, the potential high-quality image \hat{x} can be obtained by solving a MAP(maximum a posteriori) problem:

$$\hat{x} = \arg \max_x \log p(y|x) + \log p(x). \quad (2)$$

However, designing such priors is a challenging task and often not generalizable. Recently, stimulated by the success of deep learning for high-level vision tasks, numerous deep models [6]–[13] have been developed to tackle low-level vision tasks. With large-scale data, deep models such as Convolutional Neural Networks(CNNs) and Transformer can implicitly learn more general priors by capturing natural image statistics and achieving state-of-the-art(SOTA) performance in image restoration.

The performance gain of deep learning methods over the others is primarily attributed to its model design. Numerous network modules and functional units for image restoration have been investigated to design various models in recent years, including encoder-decoder [10], [11], multi-stage network [8], [13]–[15], dual network [16]–[19], recursive residual [20], [21] and various transformer improvements [12], [22]–[24]. Despite their good performance, these methods suffer from high system complexity, it often takes a long time and a lot of video memory to run a model with a large number of parameters.

Based on the above facts, a natural question arises: Is it possible to summarize the advantages of the above network structure and propose a neural network with computational costs to get considerable results? To this end, we analyze the characteristics of the above network structure and identify the architectural bottlenecks that hamper their performance. First, the structure of the encoder-decoder can learn the contextualized features but is unreliable in preserving spatial image details. Second, the multi-stage network can learn multi-scale contextual information and preserve fine spatial details, while may yield sub-optimal results. Third, the dual network is more flexible for low-level vision tasks, yet the results are not good. What's more, in order to avoid gradient disappearance, many network structures use the recursive residual but only as a sub-network. Finally, despite showing outstanding performance, existing Transformer backbones for image restoration still suffer from serious defects, such as self-attention computation.

To address the above issues, we propose a mixed hierarchy image restoration network architecture, named as MHNet. Our approach is universal, as it can be adapted for generic image restoration problems. Specifically, (1) We draw lessons from the idea of multi-stage and dual networks and use multiple subnetworks to extract features, the first hierarchy uses an encoder-decoder to learn multi-scale contextual information, while the last hierarchy maintains fine spatial details by

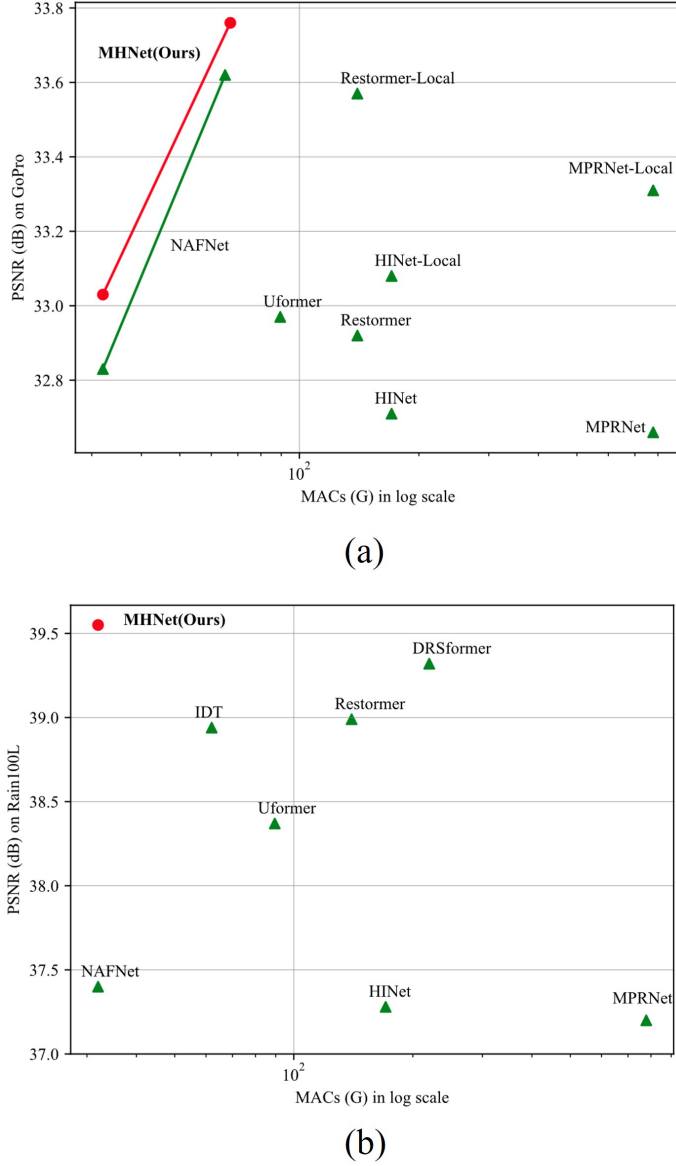


Fig. 1. Computational cost vs. PSNR of models on Image Deblurring (top) and Image Deraining (bottom) tasks. Our MHNet achieve the SOTA performance with up to 85% of cost reduction on Image Deraining .

operating on the full-resolution. (2) In order to incorporate information exchange between different hierarchies, we design an adaptive feature fusion mechanism (AFFM) to selectively aggregates spatially-precise details and complementary contextual information. (3) We learn the attention mechanism of the transformer and propose a selective multi-head attention mechanism (SMAM) to adaptively retain the most crucial attention scores, thereby facilitating better feature aggregation. As shown in Figure 1, our MHNet model achieves state-of-the-art performance while being computationally efficient in comparison to existing methods.

The main contributions of this work are:

- 1) By analyzing the SOTA methods and extracting their essential components, we proposed a novel mixed hierarchy method that efficiently generates a restored image

- that is rich in contextual and accurate in spatial detail.
- 2) We design an adaptive feature fusion mechanism (AFFM) across hierarchy that effectively combines spatially-precise details and complementary contextual information.
 - 3) We propose a selective multi-head attention mechanism (SMAM) as the encoder-decoder middle block that is capable of aggregating the most crucial information contained in the feature maps captured by convolution.
 - 4) We use the nonlinear activation free block as our base block to reduce the system complexity.
 - 5) We demonstrate the versatility of MHNet by setting new state-of-the-art on 6 synthetic and real-world datasets for various restoration tasks (image deraining and deblurring) while maintaining low complexity. Further, we provide detailed analysis, qualitative results, and generalization tests.

II. RELATED WORK

A. Image Restoration

Image restoration aims to restore a degraded image to a clean one, it is split into a large number of sub-problems, for image deblurring, and image deraining among others. Early restoration approaches are usually defined by hand-crafted priors that narrowed the ill-posed nature of the problems by reducing the set of plausible solutions, such as total variation [1], [25], sparse coding [26]–[28] self-similarity [29], [30], gradient prior [31], [32], etc. With the rapid development of deep learning, numerous works based on deep learning have gained great popularity for image restoration, and achieve SOTA results [8], [13], [22]–[24], [33]. Although the above methods achieve a considerable result, they suffer from high system complexity and often takes a lot of video memory to run a model with a large number of parameters.

B. Encoder-Decoder Approaches

In recent years, encoder-decoder have gained great attention from researchers in the field of image restoration. There are many variations of encoder-decoder, such as using multiple layers of convolution and deconvolution operators [34], cascading of the network input into intermediate layers [35], many compositions of the encoder-decoder sub-networks [36], deepen the network depth, and introducing the capsule network [37]. By learning end-to-end mappings from corrupted images to the original ones, this methods [8], [23], [38] achieve SOTA results on image restoration. However, the encoder-decoder approach is not reliable in preserving spatial image details.

C. Multi-Stage Approaches

Multi-stage approaches divide the task of image restoration into multiple stages by employing light-weight subnetworks [8], [14], [15], [39]–[42]. In this way, spatial details and high-level contextualized information is gradually captured, the image restoration process becomes more controlled. However, the multi-stage model parameters are too large, the MACs are low, may yield sub-optimal results, and the loss of *nan* is easy to occur.

D. Dual Networks

Dual Networks have two parallel branches, which respectively estimate the structure and detail components of the target signals from the input, and then reconstruct the final results according to the specific tasks formulation module. [16] first proposed the DualCNN framework, which has inspired the following work, including image dehazing [43]–[45], image deraining [46], image denoising [47], and image super-resolution/deblurring [18].

E. Vision Transformer

Due to the content-dependent global receptive field, the transformer architecture [48] has recently gained much popularity in the high-level computer vision community, such as image classification, segmentation, object detection [49]–[52]. After the impressive performance on high-level vision tasks, researchers have been started to try to use it in image restoration [12], [23], [24], [53]–[57]. [54] proposed a strong baseline model named SwinIR. [23] also proposed an efficient Transformer model using a U-net structure named Restormer and achieved state-of-the-art results on several image restoration tasks. However, the state-of-the-art results rely on a large number of parameters and heavy computation (over 115.5M parameters), and high MACs, which are bad for devices with limited resources.

III. METHOD

Our original intention is to look for a network structure that summarizes the advantages of the existing network structure and gets considerable results with lower computational costs. The overview of the proposed framework MHNet for image restoration, shown in Figure. 2, consists of two hierarchy structures. The first hierarchy is based on encoder-decoder subnetworks that learn the contextualized features with broad context. And the next hierarchy employs a subnetwork that operates on the full resolution to retain local information.

Instead of simply employing the U-Net as the encoder-decoder network, we're based on [10] research, replacing or removing the nonlinear activation function by multiplication and using a simple network structure. What's more, we replace convolution with global self-attention in the middle block. Such a hybrid design can aggregate more information and let attention work on smaller resolutions generated by having convolutions do the spatial downsampling. Furthermore, we introduce a feature fusion mechanism to incorporate information exchange between different hierarchies.

Overall Pipeline. Given a degraded image $\mathbf{I} \in \mathbb{R}^{H \times W \times 3}$, MHNet first applies a convolution to obtain low-level features $\mathbf{X}_0 \in \mathbb{R}^{H \times W \times C}$. Next, the \mathbf{X}_0 pass through a encoder-decoder network, yielding encoder features $\mathbf{E}[\mathbf{X}_{e1}, \mathbf{X}_{e2}, \mathbf{X}_{e3}, \mathbf{X}_{e4}]$ and decoder features $\mathbf{D}[\mathbf{X}_{d1}, \mathbf{X}_{d2}, \mathbf{X}_{d3}, \mathbf{X}_{d4}]$, respectively. In order to assist the image restoration, the encoder features \mathbf{E} are added with the decoder features \mathbf{D} via skip connections. Then, we input the features \mathbf{X}_1 of the concatenation of \mathbf{X}_0 and \mathbf{X}_{d4} into N number of full resolution subnetwork (FRSNet), yielding deep features $\mathbf{X}_d \in \mathbb{R}^{H \times W \times C}$. It is worth noting that we introduce

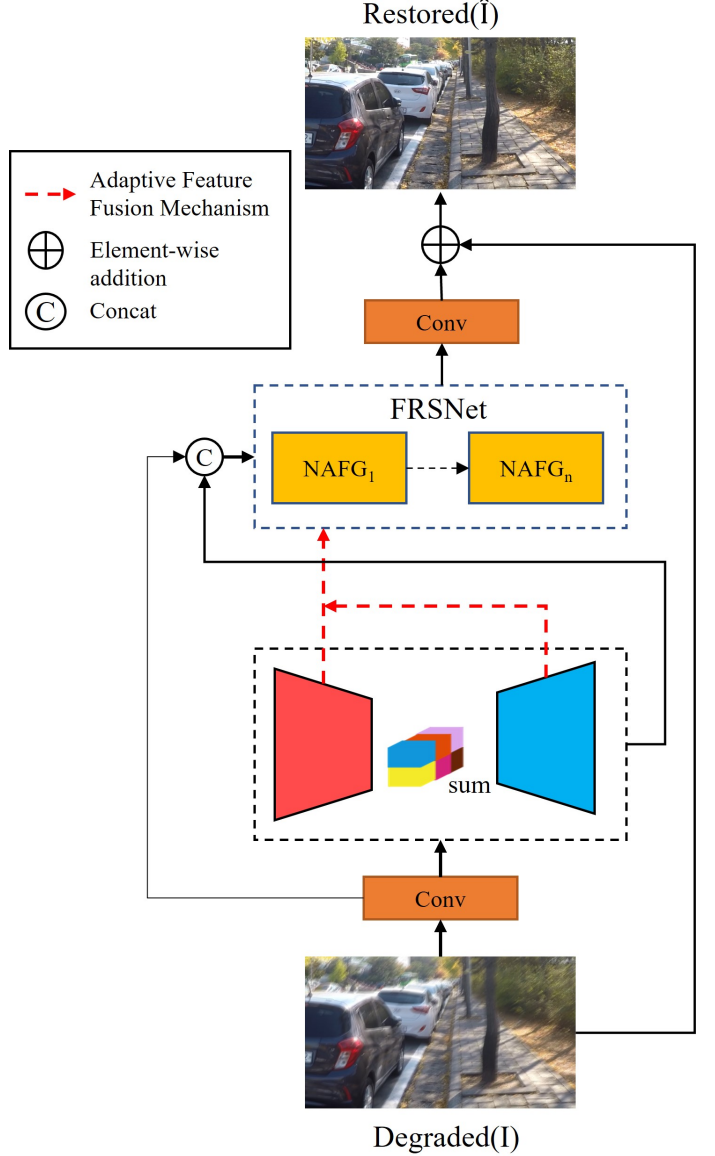


Fig. 2. Architecture of MHNet for image restoration.

the feature fusion module between the encoder-decoder and FRSNet. Finally, we apply convolution to the refined features to generate residual image $\mathbf{X} \in \mathbb{R}^{H \times W \times 3}$ to which degraded image is added to obtain the restored image: $\hat{\mathbf{I}} = \mathbf{X} + \mathbf{I}$. We optimize the proposed network using PSNR loss :

$$PSNR = 10 \cdot \log_{10} \cdot \frac{(2^n - 1)^2}{\|\hat{\mathbf{I}} - \mathbf{I}\|^2} \quad (3)$$

where $\hat{\mathbf{I}}$ denotes the ground-truth image.

A. Mix Hierarchy Network

Existing methods for image restoration typically use the following architecture designs: 1). The single-stage encoder-decoder, by using CNN or Transformer [23], [54], [58]–[60] first gradually map the input to low-resolution representations, and then progressively apply reverse mapping to recover the

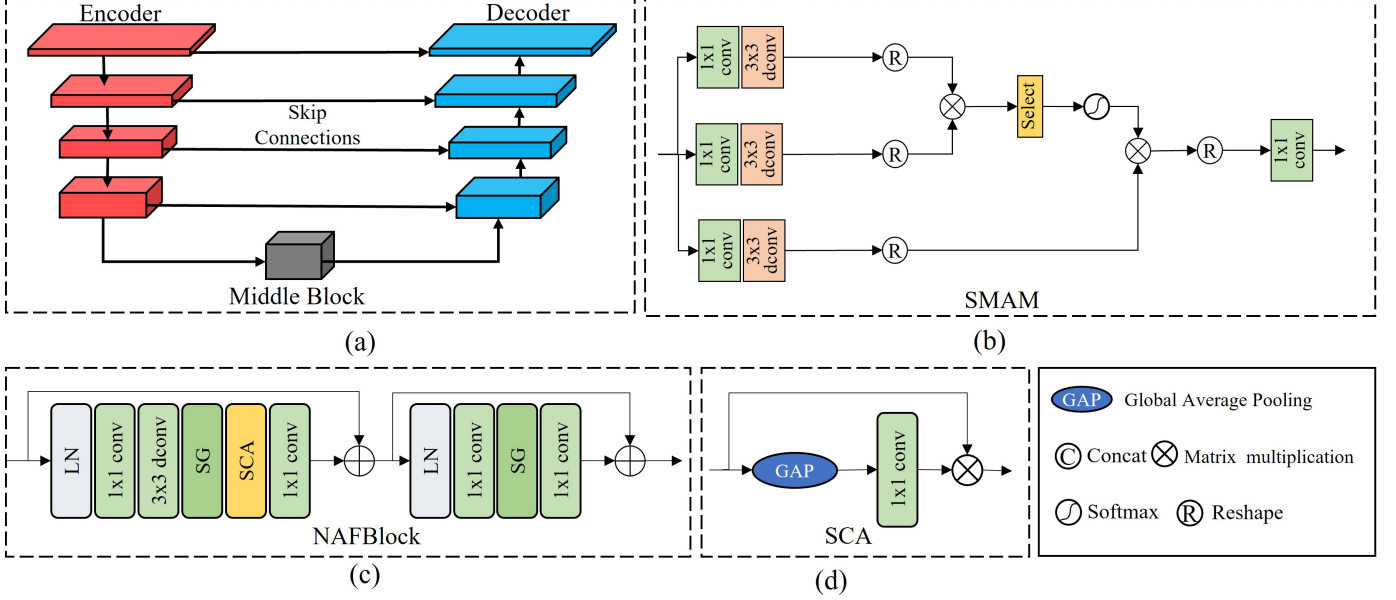


Fig. 3. (a) Encoder-decoder subnetwork. (b) Selective multi-head attention mechanism (SMAM) (c) The architecture of nonlinear activation free block (NAFBlock) [10]. (d) Simplified Channel Attention (SCA).

original resolution. Although these models effectively encode multi-scale contextualized information, they tend to sacrifice spatial details. Two branches for spatial details and contextualized information. These networks divide the task of image restoration into estimating the structure and detail components of the target signals from the input by employing a light-weight sub-network [8], [15], [42]. In this way, spatial details and contextualized information is gradually captured, and the image restoration process becomes more controlled. However, these model parameters are too large, the MACs are high, may yield sub-optimal results, and the loss of *nan* is easy to occur. Based on the merits of these structure designs, we propose a mix hierarchy network where earlier use the encoder-decoder network to capture context information and later operates on the full resolution that preserves spatial detail.

B. Encoder-Decoder Subnetwork

As shown in Figure 3(a), we adopt the classic U-shaped architecture with skip-connections as our encoder-decoder subnetwork and add or replace the following components.

Nonlinear Activation Free Block (NAFBlock). In order to reduce computing resources and speed up computing, we adopt the nonlinear activation free block (NAFBlock) [10] as our base block in our MHNet. Fig 3(c) illustrates the process of obtaining an output Y from an input X using Layer Normalization (LN), Convolution, Simple Gate (SG), and Simplified Channel Attention (SCA). Express as follows:

$$\begin{aligned} X_1 &= X + f_{1 \times 1}^c(SCA(SG(f_{3 \times 3}^{dwc}(f_{1 \times 1}^c(LN(X)))))) \\ Y &= X_1 + f_{1 \times 1}^c(SG(f_{1 \times 1}^c(LN(X_1)))) \\ SCA &= X_{f3} \cdot f_{1 \times 1}^c(GAP(X_{f3})) \\ SG &= X_{f1} \cdot X_{f2} \end{aligned} \quad (4)$$

where $f_{1 \times 1}^c$ represents 1×1 convolution, $f_{3 \times 3}^{dwc}$ denotes the 3×3 depth-wise convolution, and GAP is the global average pooling. For a given input X_{f0} , SG initially splits it into two features $X_{f1}, X_{f2} \in \mathbb{R}^{H \times W \times \frac{C}{2}}$ along channel dimension. Subsequently, SG calculates the X_{f1}, X_{f2} using a linear gate. For a more intuitive representation, we illustrate $SCA(\cdot)$ in Fig.3(d).

Selective Multi-head Attention Mechanism (SMAM). Due to the limited receptive field, there are many hindrances by using CNN for image restoration. However, there also are a few challenges when using self-attention in vision, such as the overheads for training. The computation on a global scale results in a quadratic complexity in relation to the number of tokens as shown in Eq. 5, rendering it inadequate for the representation of high-resolution images.

$$O_{MSA} = 4hwC^2 + 2(hw)^2C \quad (5)$$

Furthermore, the conventional self-attention approach necessitates the computation of attention maps for all query-key pairs, posing challenges for image restoration due to potential noisy interactions among irrelevant features. To this end, we design a selective multi-head attention mechanism (SMAM) (see Figure 3(b)) as the middle block of the encoder-decoder. SMAM allows for the adaptive retention of the most crucial attention scores, enabling attention to operate on smaller resolutions and thereby reducing training costs. Additionally, taking inspiration from [23], we implement SAM across channels rather than the spatial dimension to decrease time complexity.

Specifically, given an input feature $\mathbf{F} \in \mathbb{R}^{H \times W \times C}$, we first apply 1×1 convolutions and 3×3 depth-wise convolutions to aggregate channel-wise context, yielding *query*, *key* and *value* matrices $\mathbf{Q} \in \mathbb{R}^{H \times W \times C}$, $\mathbf{K} \in \mathbb{R}^{H \times W \times C}$, $\mathbf{V} \in \mathbb{R}^{H \times W \times C}$. Then we reshape $\mathbf{Q}, \mathbf{K}, \mathbf{V}$ to $\hat{\mathbf{Q}} \in \mathbb{R}^{(HW) \times \frac{C}{h} \times h}$,

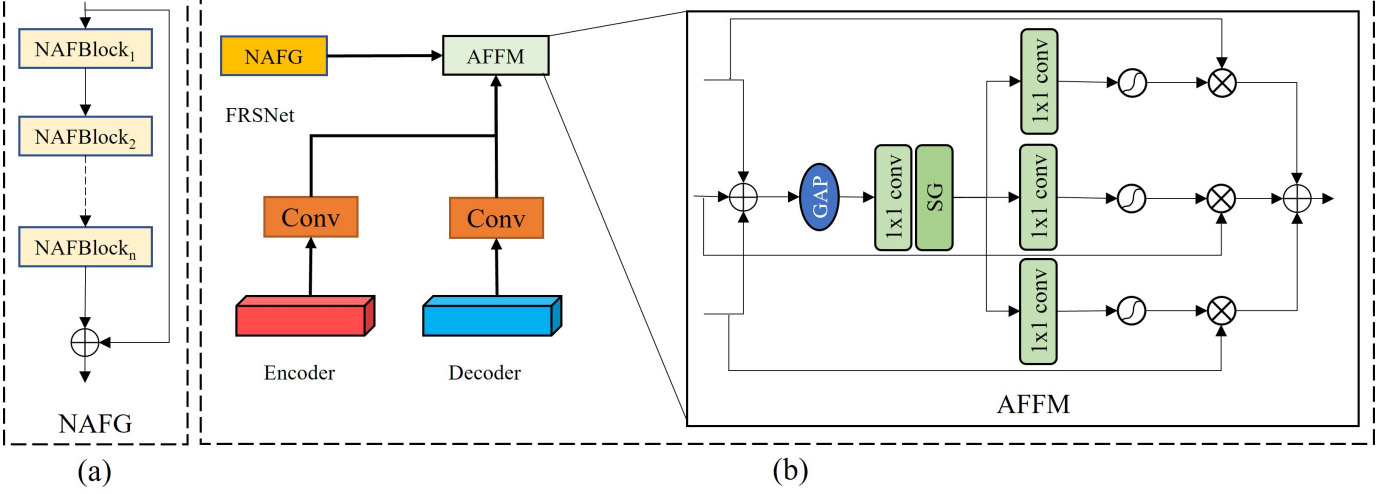


Fig. 4. (a) The architecture of nonlinear activation free block groups (NAFG). Each NAFFG further contains multiple nonlinear activation free blocks (NAFBLOCKS). (b) Adaptive feature fusion mechanism (AFFM) between an encoder-decoder subnetwork and FRSNet.

$\hat{\mathbf{K}} \in \mathbb{R}^{(HW) \times \frac{C}{h} \times h}$, $\hat{\mathbf{V}} \in \mathbb{R}^{(HW) \times \frac{C}{h} \times h}$, where h is the number of head. Subsequently, we compute similarities between \hat{Q} and \hat{K}^T , selectively choosing the most crucial attention scores for softmax computation. The probabilities of other elements are then replaced with 0. The entire self-attention procedure of the developed SMAM is formulated as:

$$SMAM(\hat{\mathbf{Q}}, \hat{\mathbf{K}}, \hat{\mathbf{V}}) = \text{Softmax}\left(\lambda\left(\frac{\hat{Q}\hat{K}^T}{\beta}\right)\right)\hat{V} \quad (6)$$

where β is a learning scaling parameter used to adjust the magnitude of the dot product of \hat{Q} and \hat{K} prior to the application of the softmax function. And $\lambda(\cdot)$ is the trainable selection operator:

$$\lambda(\gamma) = \begin{cases} \gamma & \text{if } \gamma \geq t \\ 0 & \text{otherwise.} \end{cases} \quad (7)$$

Finally, we reshape the attention matrix back to its original dimensions of $\mathbb{R}^{H \times W \times C}$. And the computation change from quadratic complexity \mathcal{O}_{MSA} to linear complexity \mathcal{O}_{SMAM} .

$$\mathcal{O}_{SMAM} = 5hwC^2 + hwC \quad (8)$$

C. Full Resolution Subnetwork (FRSNet)

As we mentioned before, we use the encoder-decoder subnetwork to capture context information. While recovering images demands a complex balance between spatial details and contextualized information, thus we introduce the full resolution subnetwork (FRSNet) to preserve fine details from the degraded image to the restored image. It consists of N numbers nonlinear activation free block groups (NAFGs), each of which further contains NAFBlocks. Figure 4(a) shows the architecture of NAFFG. Formally, let given a features \mathbf{X}_i as the input of the $i + 1$ -th NAFFG, $\mathbf{X}_{ei} \in \mathbb{R}^{\frac{H}{i^2} \times \frac{W}{i^2} \times i^2 C}$, $\mathbf{X}_{di} \in \mathbb{R}^{\frac{H}{i^2} \times \frac{W}{i^2} \times i^2 C}$ be the output in the $i + 1$ -th level encoder

decoder respectively ($i = 1, 2, 3, 4$). The encoding procedures of NAFFG can be defined as:

$$\begin{aligned} NAFFG(X_i) &= X_i + NAFBlock_{l-1}(X_i) \\ X_1 &= f_{1 \times 1}^c([X_0, X_{d4}]) \\ X_{i+1} &= AFFM(NAFFG(X_i), X_{di}, X_{ei}) \end{aligned} \quad (9)$$

where $[\cdot]$ represents the channel-wise concatenation, $NAFBlock_{l-1}$ is the l number NAFBlocks, and $AFFM(\cdot)$ denotes the adaptive feature fusion mechanism which will be described below.

D. Adaptive Feature Fusion Mechanism (AFFM)

The integration of information exchange across various hierarchies stands as a pivotal aspect of our mixed hierarchy architecture. Commonly employed methods [8], [14], [15] for feature aggregation involve simplistic concatenation or summation. Nevertheless, these options offer limited expressive. Inspired by the [9], [61], we propose the adaptive feature fusion mechanism (AFFM) for integrating features from distinct hierarchies. AFFM employs a self-attention mechanism, illustrated in Figure 4(b), to selectively combine spatially-precise details and rich contextual information. Specifically, given the output features of the encoder-decoder, denoted as X_{ei} and X_{di} , along with the output feature of the i -th NAFFG, denoted as X_i , we initially employ PixelShuffle and convolution operations to align the channel count and feature map size of X_{ei} and X_{di} with those of X_i . Subsequently, we combine them using an element-wise sum as follows:

$$\begin{aligned} \hat{X}_{ei} &= f_{1 \times 1}^c(PS(X_{ei})) \\ \hat{X}_{di} &= f_{1 \times 1}^c(PS(X_{di})) \\ X_S &= X_i + \hat{X}_{ei} + f\hat{X}_{di} \end{aligned} \quad (10)$$

where $PS(\cdot)$ represents the PixelShuffle to upsample the X_{ei} and X_{di} .

Next, we perform global average pooling (GAP) across the spatial dimensions of $X_S \in \mathbb{R}^{H \times W \times C}$ to compute channel-wise statistics. Subsequently, we apply a channel-downscaling

TABLE I

IMAGE DERAINING RESULTS. THE BEST AND SECOND BEST SCORES ARE **HIGHLIGHTED** AND UNDERLINED. OUR MHNET IS BETTER THAN THE STATE-OF-THE-ART BY 0.32 dB.

Methods	Test100 [62]		Test1200 [63]		Rain100H [64]		Rain100L [64]		Average	
	PSNR \uparrow	SSIM \uparrow								
DerainNet [65]	22.77	0.810	23.38	0.835	14.92	0.592	27.03	0.884	22.48	0.796
SEMI [66]	22.35	0.788	26.05	0.822	16.56	0.486	25.03	0.842	22.88	0.744
DIDMDN [67]	22.56	0.818	29.65	0.901	17.35	0.524	25.23	0.741	24.58	0.770
UMRL [68]	24.41	0.829	30.55	0.910	26.01	0.832	29.18	0.923	28.02	0.880
RESCAN [15]	25.00	0.835	30.51	0.882	26.36	0.786	29.80	0.881	28.59	0.857
PreNet [14]	24.81	0.851	31.36	0.911	26.77	0.858	32.44	0.950	29.42	0.897
MSPFN [63]	27.50	0.876	32.39	0.916	28.66	0.860	32.40	0.933	30.75	0.903
MPRNet [8]	30.27	0.907	32.91	0.916	30.51	0.890	37.20	0.965	32.73	0.921
SPAIR [69]	30.35	<u>0.909</u>	33.04	0.922	30.95	0.893	37.30	0.978	32.91	0.926
HINet [13]	30.29	0.906	33.05	0.919	30.65	0.894	37.28	0.970	32.81	0.922
U ² Former [70]	-	-	33.48	0.926	30.87	0.893	39.31	0.982	-	-
MDARNet [71]	28.98	0.892	33.08	0.919	29.71	0.884	35.68	0.961	31.86	0.914
SDLNet [72]	-	-	-	-	30.83	0.891	39.52	0.981	-	-
Restormer [23]	31.32	0.910	33.19	0.926	31.06	0.895	38.99	0.975	33.64	<u>0.926</u>
DRSformer [55]	-	-	-	-	31.13	<u>0.903</u>	<u>40.01</u>	<u>0.989</u>	-	-
NAFNet [10]	30.25	0.908	32.92	0.917	30.40	0.891	37.40	0.964	32.73	0.921
MHNet(Ours)	31.25	0.901	<u>33.45</u>	<u>0.925</u>	<u>31.08</u>	<u>0.899</u>	40.04	<u>0.985</u>	33.96	0.928

convolution layer and SG to generate a compact feature representation. This compact feature is then passed through three parallel channel-upscaling convolution layers to create global feature descriptors. This descriptors applies the softmax function to yield attention score that we use to adaptively modify the features X_i , X_{ei} and X_{di} , respectively. Finally, we use element-wise addition to fuse this features to obtain X_{i+1} . The entire procedure of AFFM is defined as:

$$\begin{aligned}
 X_S^c &= SG(f_{1 \times 1}^c(GAP(X_S))) \\
 X_e^d &= softmax(f_{1 \times 1}^c(X_S^c)) \\
 X_d^d &= softmax(f_{1 \times 1}^c(X_S^c)) \\
 X_x^d &= softmax(f_{1 \times 1}^c(X_S^c)) \\
 X_{i+1} &= X_e^d \cdot \hat{X}_{ei} + X_d^d \cdot \hat{X}_{di} + X_x^d \cdot X_i
 \end{aligned} \tag{11}$$

The proposed AFFM offers several advantages. Firstly, it mitigates feature loss during the up and down sampling in the encoder-decoder, thereby enhancing feature information at the subsequent hierarchy and promoting more stable model training. Moreover, the dynamic adjustment in the fusion process ensures the integration of the most useful information, enhancing the aggregated features for more effective high-quality image reconstruction.

IV. EXPERIMENTS

We evaluate the proposed MHNet on benchmark datasets for two image restoration tasks, including **(a)** image deraining, and **(b)** image deblurring.

A. Implementation Details

We train the proposed MHNet without any pre-training and separate models for different image restoration tasks. In the encoder-decoder subnetwork, we employ 4 layers of encoder-decoder and 1 middle block. We apply [1, 1, 1, 28] NAFBlock at each scale of the encoder, [1, 1, 1, 1] NAFBlock at each scale of the decoder, and 8 heads for the SMAM. In the full resolution subnetwork, we use 4 NAFFGs, each of which further

contains 8 NAFFBlocks. Depending on the task complexity, we scale the network width by setting the number of channels to 32 for deraining, and 32, 64 for deblurring. We train models with Adam [73] optimizer ($\beta_1 = 0.9$, $\beta_2 = 0.999$) and PSNR loss for 4×10^5 iterations with the initial learning rate 5×10^{-4} gradually reduced to 1×10^{-7} with the cosine annealing [74]. We extract patches of size 256×256 from training images, and the batch size is set to 32. For data augmentation, we perform horizontal and vertical flips.

B. Image Deraining Results

Following the prior work [8], [63], [69], we computer PSNR/SSIM scores using the Y channel in YCbCr color space for image deraining task. As Table. I shows, our method gains consistent and significant performance gains over existing approaches. Compared to our baseline network NAFNet [10], our method achieves 1.23 dB improvement when averaged across all datasets. The improvements on some datasets are as large as 2.64 dB. e.g., Rain100L [64]. Compared to the recent best algorithm DRSformer [55], we obtain competitive results. Compared to the Resformer [23], our method achieves 0.32 dB improvement when averaged across all datasets. In comparison to our baseline network, NAFNet [10], our method demonstrates a notable 1.23 dB improvement on average across all datasets, with some datasets showing improvements as substantial as 2.64 dB (e.g., Rain100L [64]). Compared to Resformer [23], our approach achieves a 0.32 dB improvement on average across all datasets. Furthermore, compared to the state-of-the-art algorithm DRSformer [55], our method yields competitive results.

Figure. 5 shows our MHNet is effective in removing rain streaks of different orientations and magnitudes while effectively preserving the structural content.

C. Image Deblurring Result

As shown in Table. II, we evaluated the performance of image deblurring approaches on the GoPro [75] and HIDE [76]

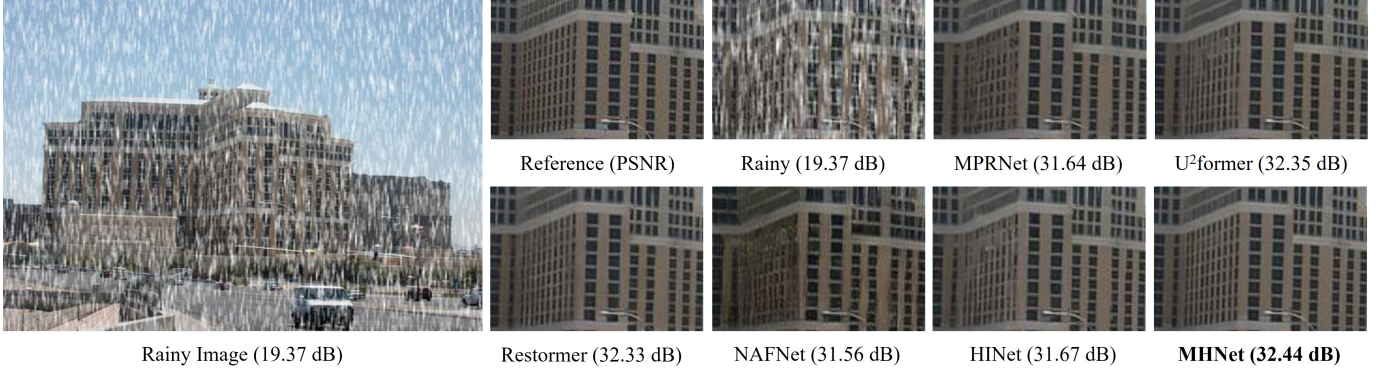


Fig. 5. **Image deraining** example. The outputs of the MHNet exhibit no traces of rain streaks on both image sample. MHNet also recovers the most detailed images.

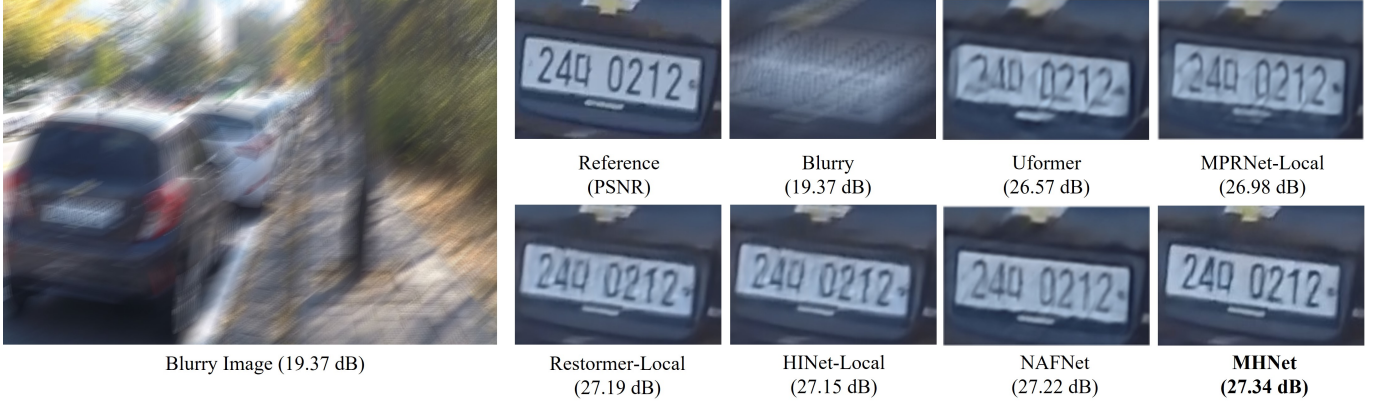


Fig. 6. **Image deblurring** example on the GoPro dataset [75]. Compared to the state-of-the-art methods, our MHNet restores sharper and perceptually-faithful images.

datasets. Overall, our MHNet outperformed other methods, with a performance gain of 0.32dB when averaging across all datasets [75], [76]. Specifically, compared to our baseline network NAFNet [10], we improve 0.2 dB and 0.14 dB at 32 and 64 number of channels, respectively. Compared with previous best method, Restormer-local [23], we improve 0.19 dB on the GoPro [75] dataset and 0.44 dB on HIDE [76] dataset. In comparison to the recent algorithm MSFS-Net-Local [77], our MHNet achieves a 0.47 dB improvement on average across all datasets. Noted that, even though our network is trained solely on the GoPro [75] dataset, it still achieves state-of-the-art results (31.93 dB in PSNR) on the HIDE [76] dataset. This demonstrates its impressive generalization capability. Figure. 6 shows some of the images deblurred by the evaluation method, our model recovered clearer images and was closer to ground truth.

Furthermore, in order to demonstrate the applicability of our approach in road scenarios, we utilized the CamVid and KITTI datasets, both of which are open datasets featuring road scenes, to generate a dataset of motion-blurred image pairs through a random motion blur generation method. The results are shown in Table. III, our method outperforms the state-of-the-art methods.

TABLE II
IMAGE DEBLURRING RESULTS. THE PROPOSED M3SNET IS TRAINED ONLY ON THE GOPRO DATASET BUT ACHIEVES A 0.32 dB IMPROVEMENT OVER THE STATE OF THE ART ON THE AVERAGE OF THE EFFECTS ON BOTH DATASETS.

Methods	GoPro [75]		HIDE [76]		Average	
	PSNR \uparrow	SSIM \uparrow	PSNR \uparrow	SSIM \uparrow	PSNR \uparrow	SSIM \uparrow
DeblurGAN [78]	28.70	0.858	24.51	0.871	26.61	0.865
Nah <i>et al.</i> [75]	29.08	0.914	25.73	0.874	27.41	0.894
DeblurGAN-v2 [60]	29.55	0.934	26.61	0.875	28.08	0.905
SRN [39]	30.26	0.934	28.36	0.915	29.31	0.925
Gao <i>et al.</i> [79]	30.90	0.935	29.11	0.913	30.01	0.924
DBGAN [80]	31.10	0.942	28.94	0.915	30.02	0.929
MT-RNN [81]	31.15	0.945	29.15	0.918	30.15	0.932
DMPHN [42]	31.20	0.940	29.09	0.924	30.15	0.932
Suin <i>et al.</i> [82]	31.85	0.948	29.98	0.930	30.92	0.939
SPAIR [69]	32.06	0.953	30.29	0.931	31.18	0.942
MIMO-UNet++ [83]	32.45	0.957	29.99	0.930	31.22	0.944
MPRNet [8]	32.66	0.959	30.96	0.939	31.81	0.949
MPRNet-local [8]	33.31	0.964	31.19	0.945	32.25	0.955
Restormer [23]	32.92	0.961	31.22	0.942	32.07	0.952
Restormer-local [23]	33.57	0.966	31.49	0.945	32.53	0.956
Uformer [12]	32.97	0.967	30.83	0.952	31.90	0.960
HINet [13]	32.71	-	-	-	-	-
HINet-local [13]	33.08	0.962	-	-	-	-
MSFS-Net [77]	32.73	0.959	31.05	0.941	31.99	0.950
MSFS-Net-local [77]	33.46	0.964	31.30	0.943	32.38	0.954
NAFNet-32 [10]	32.83	0.960	-	-	-	-
NAFNet-64 [10]	33.62	0.967	-	-	-	-
MHNet-32 (ours)	33.03	0.965	31.02	0.949	32.03	0.957
MHNet-64 (ours)	33.76	0.969	31.93	0.951	32.85	0.960

TABLE III

COMPARING THE IMAGE QUALITY ACHIEVED BY THE PROPOSED METHOD WITH STATE-OF-THE-ART TECHNIQUES, WE EVALUATED THE PERFORMANCE USING METRICS SUCH AS SNR, PSNR, AND SSIM. THE TERM "BLURRED" REFERS TO THE DIFFERENCE IN THESE METRICS BETWEEN THE MOTION-BLURRED IMAGE AND THE ORIGINAL GROUND-TRUTH IMAGE.

Methods	SNR	PSNR	SSIM
Blurred	11.86	19.87	0.57
DeblurGAN-v2 [60]	13.61	21.63	0.67
MPRNet [8]	14.99	23.00	0.76
HINet [13]	15.15	23.16	<u>0.75</u>
MIMO-UNet++ [83]	14.34	22.36	0.73
MHNet(our)	15.42	23.19	<u>0.75</u>

TABLE IV

ABLATION STUDY ON INDIVIDUAL COMPONENTS OF THE PROPOSED MHNET.

Mix Network	SMAM	AFFM	PSNR
U-Net + U-Net	✗	✗	32.66
FRSNet + FRSNet	✗	✗	31.88
U-Net + FRSNet	✗	✗	32.74
U-Net + FRSNet	✓	✗	32.85
U-Net + FRSNet	✗	✓	32.99
U-Net + FRSNet	✓	✓	33.03

D. Ablation Studies

The ablation studies are conducted on image deblurring (GoPro [75]) to analyze the impact of each of our model components. Next, we describe the impact of each component.

Choices of subnetwork. Our goal is to find two subnetwork models to capture spatial details and context information respectively and construct a mixed network to achieve image restoration. Therefore, we tested the effect of using different subnetworks on the experimental results. As the Table IV shown, we using the U-Net + FRSNet leads to better performance (33.03 dB) as compared to employing the same design. This shows that combining the encoder-decoder structure with a high-resolution subnetwork can achieve a balance between spatial details and high-level contextualized information while recovering images.

Adaptive Feature Fusion Mechanism (AFFM). The incorporation of information exchange across diverse hierarchies is a crucial aspect of our mixed hierarchy architecture. We analyze the feature aggregation strategy in Table V. It shows that the AFFM achieves improvements of 0.18 dB, 0.16 dB, and 0.12 dB compared to summation, concatenation and CSFF [8]. We also verify that the effect of feature fusion mechanism for hierarchy architecture. As indicated in Table IV, the removal of the AFFM results in a substantial performance degradation, dropping from 32.99 dB to 32.74 dB.

Selective Multi-head Attention Mechanism (SMAM). The proposed SMAM as the encoder-decoder middle block is

TABLE V

THE INFLUENCE OF DIFFERENT FEATURE FUSION MECHANISM.

	Sum	Concat	CSFF [8]	AFFM
PSNR	32.85	32.87	32.91	33.03

TABLE VI
THE INFLUENCE OF DIFFERENT ATTENTION MECHANISM.

	FASA [56]	W-MSA [12]	MDTA [23]	AFFM
PSNR	32.93	32.87	32.99	33.03

TABLE VII
THE EVALUATION OF MODEL COMPUTATIONAL COMPLEXITY. THIS IS CONDUCTED WITH AN INPUT SIZE OF 256×256 , ON AN NVIDIA 1060 GPU.

Method	PSNR	Params(M)	MACs(G)
MIMO-UNet++ [83]	32.68	16.1	1235
MPRNet [8]	32.66	20.1	778.2
MPRNet-local [8]	33.31	20.1	778.2
HINet [13]	32.77	88.7	170.7
Restormer [23]	32.92	26.13	140
Restormer-local [23]	33.57	26.13	140
Uformer [12]	32.97	50.88	89.5
NAFNet-32 [10]	32.83	17.1	32
NAFNet-64 [10]	33.62	68	65
MHNet-32 (ours)	33.03	16.9	32
MHNet-64 (ours)	33.76	67	67

used to aggregate the most crucial information contained in the feature maps captured by convolution. To examine the effect of SMAM, we substitute the attention mechanism in MHNet with several SOTA approaches, including FASA [56], W-MSA [12], and MDTA [23]. As shown in Table. VI, compared with FASA, W-MSA, and MDTA, our SMAM achieves improvements of 0.1 dB, 0.16 dB, and 0.04 dB, respectively. When we examine MHNet without SMAM to assess the effect of the proposed SMAM on adaptively retain the most crucial attention scores, we find that our method achieves a 0.11 dB improvement with SMAM as shown in Table IV.

E. Resource Efficient

Many deep learning models are now becoming deeper and more complex to achieve higher accuracy. Although large models work better than small models, they are also very resource-intensive. Therefore, it is very important to design a lightweight image restoration model with high accuracy. In our work, we design a mixed hierarchy network that obtains higher accuracy with lower computing resources.

As the Table. VII shown, our MHNet gains the best performance. MIMO-UNet++ [83] has a smaller number of parameters, while MHNet using significantly fewer computational resources with MACs approximately 40 times smaller than that of MIMO-unet++. Figure 1 clearly demonstrates that our MHNet outperforms DRSformer [55] by achieving a state-of-the-art result while remarkably reducing the cost reduction by 85%. Furthermore, when compared to our baseline NAFNet [10], we achieve superior PSNR values using an equivalent computational resources. These findings highlight the highly efficient of MHNet. Moreover, through the scaling up of the model size, our MHNet achieves even better performance, highlighting the scalability of MHNet.

V. CONCLUSION

Image restoration usually demands a complex balance between spatial details and high-level contextualized information

while recovering images. In this paper, we propose a mixed hierarchy architecture that balances the competing goal by mixing two subnetworks concerned with contextual information and spatial details. Specifically, we design a selective multi-head attention mechanism as the middle block of the encoder-decoder subnetwork to aggregate the most crucial information contained in the feature maps captured by convolution. To ensure the information exchange between different hierarchies, we propose a adaptive feature fusion mechanism to selectively combine spatially-precise details and rich contextual information. In addition, to keep the size of our model lightweight and have computational efficiency, we replace or remove the nonlinear activation function with multiplication. Extensive experiments on numerous benchmark datasets demonstrate that MHNet achieves significant performance improvements with low computing resources.

REFERENCES

- [1] L. I. Rudin, S. Osher, and E. Fatemi, “Nonlinear total variation based noise removal algorithms,” *Physica D Nonlinear Phenomena*, vol. 60, no. 1-4, pp. 259–268, 1992.
- [2] P. Perona and J. Malik, “Scale-space and edge detection using anisotropic diffusion,” *IEEE Transactions on Pattern Analysis and Machine Intelligence*, vol. 12, no. 7, pp. 629–639, 2002.
- [3] S. Roth and M. J. Black, “Fields of experts: A framework for learning image priors,” in *IEEE Computer Society Conference on Computer Vision and Pattern Recognition*, 2005.
- [4] W. Dong, L. Zhang, G. Shi, and X. Wu, “Image deblurring and super-resolution by adaptive sparse domain selection and adaptive regularization,” *IEEE Transactions on Image Processing*, vol. 20, no. 7, pp. 1838–1857, 2011.
- [5] K. He, J. Sun, and X. Tang, “Single image haze removal using dark channel prior,” *IEEE Transactions on Pattern Analysis and Machine Intelligence*, 2011.
- [6] T. Dai, J. Cai, Y. Zhang, S.-T. Xia, and L. Zhang, “Second-order attention network for single image super-resolution,” in *Proceedings of the IEEE Conference on Computer Vision and Pattern Recognition*, 2019, pp. 11065–11074.
- [7] Y. Zhang, Y. Tian, Y. Kong, B. Zhong, and Y. Fu, “Residual dense network for image restoration,” pp. 1–1, 2020.
- [8] S. W. Zamir, A. Arora, S. Khan, M. Hayat, F. S. Khan, M.-H. Yang, and L. Shao, “Multi-stage progressive image restoration,” in *CVPR*, 2021.
- [9] ——, “Learning enriched features for fast image restoration and enhancement,” *IEEE Transactions on Pattern Analysis and Machine Intelligence (TPAMI)*, 2022.
- [10] L. Chen, X. Chu, X. Zhang, and J. Sun, “Simple baselines for image restoration,” *arXiv preprint arXiv:2204.04676*, 2022.
- [11] X. Chu, L. Chen, and W. Yu, “Nafssr: Stereo image super-resolution using nafnet,” in *Proceedings of the IEEE/CVF Conference on Computer Vision and Pattern Recognition (CVPR) Workshops*, June 2022, pp. 1239–1248.
- [12] Z. Wang, X. Cun, J. Bao, W. Zhou, J. Liu, and H. Li, “Uformer: A general u-shaped transformer for image restoration,” in *Proceedings of the IEEE/CVF Conference on Computer Vision and Pattern Recognition (CVPR)*, June 2022, pp. 17683–17693.
- [13] L. Chen, X. Lu, J. Zhang, X. Chu, and C. Chen, “Hinet: Half instance normalization network for image restoration,” in *Proceedings of the IEEE/CVF Conference on Computer Vision and Pattern Recognition (CVPR) Workshops*, June 2021, pp. 182–192.
- [14] D. Ren, W. Zuo, Q. Hu, P. F. Zhu, and D. Meng, “Progressive image deraining networks: A better and simpler baseline,” *2019 IEEE/CVF Conference on Computer Vision and Pattern Recognition (CVPR)*, pp. 3932–3941, 2019.
- [15] X. Li, J. Wu, Z. Lin, H. Liu, and H. Zha, “Recurrent squeeze-and-excitation context aggregation net for single image deraining,” in *European Conference on Computer Vision*, 2018.
- [16] J. Pan, S. Liu, D. Sun, J. Zhang, Y. Liu, J. Ren, Z. Li, J. Tang, H. Lu, and Y. W. a. Tai, “Learning dual convolutional neural networks for low-level vision,” in *CVPR*, 2018.
- [17] J. Pan, D. Sun, J. Zhang, J. Tang, J. Yang, Y. W. Tai, and M. H. Yang, “Dual convolutional neural networks for low-level vision,” *International Journal of Computer Vision*, 2022.
- [18] V. Singh, K. Ramnath, and A. Mittal, “Refining high-frequencies for sharper super-resolution and deblurring,” *Computer Vision and Image Understanding*, vol. 199, no. C, p. 103034, 2020.
- [19] D. Chen and M. E. Davies, “Deep decomposition learning for inverse imaging problems,” in *Proceedings of the European Conference on Computer Vision (ECCV)*, 2020.
- [20] Y. Zhang, K. Li, K. Li, L. Wang, B. Zhong, and Y. Fu, “Image super-resolution using very deep residual channel attention networks,” in *Proceedings of the European Conference on Computer Vision (ECCV)*, 2018, pp. 286–301.
- [21] S. Anwar, “Real image denoising with feature attention,” *ICCV*, 2019.
- [22] J. Zhang, Y. Zhang, J. Gu, Y. Zhang, L. Kong, and X. Yuan, “Accurate image restoration with attention retractable transformer,” in *ICLR*, 2023.
- [23] S. W. Zamir, A. Arora, S. Khan, M. Hayat, F. S. Khan, and M.-H. Yang, “Restormer: Efficient transformer for high-resolution image restoration,” in *CVPR*, 2022.
- [24] F.-J. Tsai, Y.-T. Peng, Y.-Y. Lin, C.-C. Tsai, and C.-W. Lin, “Stripformer: Strip transformer for fast image deblurring,” in *ECCV*, 2022.
- [25] T. F. Chan and C.-K. Wong, “Total variation blind deconvolution,” *IEEE transactions on image processing : a publication of the IEEE Signal Processing Society*, vol. 7 3, pp. 370–5, 1998.
- [26] L. Yu, X. Yong, and J. Hui, “Removing rain from a single image via discriminative sparse coding,” in *2015 IEEE International Conference on Computer Vision (ICCV)*, 2015.
- [27] M. Aharon, M. Elad, and A. Bruckstein, “K-svd: An algorithm for designing overcomplete dictionaries for sparse representation,” *IEEE TRANSACTIONS ON SIGNAL PROCESSING*, 2006.
- [28] J. Mairal, M. Elad, and G. Sapiro, “Sparse representation for color image restoration,” *IEEE Transactions on Image Processing*, vol. 17, no. 1, pp. 53–69, 2007.
- [29] A. Buades, B. Coll, and J. M. Morel, “A non-local algorithm for image denoising,” in *Computer Vision and Pattern Recognition, 2005. CVPR 2005. IEEE Computer Society Conference on*, 2005.
- [30] K. Dabov, A. Foi, V. Katkovnik, and K. Egiazarian, “Image denoising by sparse 3-d transform-domain collaborative filtering,” in *IEEE*, 2007, pp. 2080–2095.
- [31] S. Qi, J. Jia, and A. Agarwala, “High-quality motion deblurring from a single image,” *AcM Transactions on Graphics*, vol. 27, no. 3, pp. 1–10, 2008.
- [32] X. Li, S. Zheng, and J. Jia, “Unnatural l0 sparse representation for natural image deblurring,” in *IEEE Conference on Computer Vision and Pattern Recognition*, 2013.
- [33] X. Chu, L. Chen, , C. Chen, and X. Lu, “Improving image restoration by revisiting global information aggregation,” *arXiv preprint arXiv:2112.04491*, 2021.
- [34] X. J. Mao, C. Shen, and Y. B. Yang, “Image restoration using very deep convolutional encoder-decoder networks with symmetric skip connections,” in *NIPS*, 2016.
- [35] I. D. Mastan and S. Raman, “Multi-level encoder-decoder architectures for image restoration,” *2019 IEEE/CVF Conference on Computer Vision and Pattern Recognition Workshops (CVPRW)*, pp. 1728–1737, 2019.
- [36] J. Su, B. Xu, and H. Yin, “A survey of deep learning approaches to image restoration,” *Neurocomputing*, vol. 487, pp. 46–65, 2022.
- [37] T. Zeng, H. So, and E. Lam, “Redcap: residual encoder-decoder capsule network for holographic image reconstruction,” *Optics Express*, 2020.
- [38] S. Cheng, Y. Wang, H. Huang, D. Liu, H. Fan, and S. Liu, “NBNet: Noise Basis Learning for Image Denoising with Subspace Projection,” *CVPR*, Dec. 2021.
- [39] X. Tao, H. Gao, Y. Wang, X. Shen, J. Wang, and J. Jia, “Scale-recurrent network for deep image deblurring,” *CVPR*, 2018.
- [40] X. Fu, B. Liang, Y. Huang, X. Ding, and J. Paisley, “Lightweight pyramid networks for image deraining,” *IEEE Transactions on Neural Networks and Learning Systems*, 2018.
- [41] H. Zhang, L. Zhang, Y. Dai, H. Li, and P. Koniusz, “Event-guided multi-patch network with self-supervision for non-uniform motion deblurring,” *International Journal of Computer Vision*, pp. 1–18, 2022.
- [42] H. Zhang, Y. Dai, H. Li, and P. Koniusz, “Deep stacked hierarchical multi-patch network for image deblurring,” in *The IEEE Conference on Computer Vision and Pattern Recognition (CVPR)*, June 2019.
- [43] H. Zhu, P. Xi, V. Chandrasekhar, L. Li, and J. H. Lim, “Dehazegan: When image dehazing meets differential programming,” in *Twenty-Seventh International Joint Conference on Artificial Intelligence IJCAI-18*, 2018.

- [44] T. Guo, X. Li, V. Cherukuri, and V. Monga, “Dense scene information estimation network for dehazing,” in *2019 IEEE/CVF Conference on Computer Vision and Pattern Recognition Workshops (CVPRW)*, 2019.
- [45] A. Yang, H. Wang, Z. Ji, Y. Pang, and L. Shao, “Dual-path in dual-path network for single image dehazing,” in *Twenty-Eighth International Joint Conference on Artificial Intelligence IJCAI-19*, 2019.
- [46] L. I. Siyuan, W. Ren, J. Zhang, J. Yu, and X. Guo, “Fast single image rain removal via a deep decomposition-composition network,” 2018.
- [47] C. Tian, Y. Xu, W. Zuo, B. Du, C.-W. Lin, and D. Zhang, “Designing and training of a dual cnn for image denoising,” *Knowledge-Based Systems*, vol. 226, p. 106949, 2021.
- [48] A. Vaswani, N. Shazeer, N. Parmar, J. Uszkoreit, L. Jones, A. N. Gomez, L. Kaiser, and I. Polosukhin, “Attention is all you need,” *arXiv*, 2017.
- [49] M. V. Conde and K. Turgutlu, “Clip-art: Contrastive pre-training for fine-grained art classification,” in *Proceedings of the IEEE/CVF Conference on Computer Vision and Pattern Recognition (CVPR) Workshops*, June 2021, pp. 3956–3960.
- [50] A. Dosovitskiy, L. Beyer, A. Kolesnikov, D. Weissenborn, X. Zhai, T. Unterthiner, M. Dehghani, M. Minderer, G. Heigold, S. Gelly, J. Uszkoreit, and N. Houlsby, “An image is worth 16x16 words: Transformers for image recognition at scale,” *ICLR*, 2021.
- [51] Z. Liu, Y. Lin, Y. Cao, H. Hu, Y. Wei, Z. Zhang, S. Lin, and B. Guo, “Swin transformer: Hierarchical vision transformer using shifted windows,” in *ICCV 2021*, October 2021.
- [52] X. Chen, C.-J. Hsieh, and B. Gong, “When vision transformers outperform resnets without pretraining or strong data augmentations,” *arXiv preprint arXiv:2106.01548*, 2021.
- [53] M. V. Conde, U.-J. Choi, M. Burchi, and R. Timofte, “Swin2SR: SwinV2 transformer for compressed image super-resolution and restoration,” in *Proceedings of the European Conference on Computer Vision (ECCV) Workshops*, 2022.
- [54] J. Liang, J. Cao, G. Sun, K. Zhang, L. Van Gool, and R. Timofte, “SwinIR: Image restoration using swin transformer,” *arXiv preprint arXiv:2108.10257*, 2021.
- [55] X. Chen, H. Li, M. Li, and J. Pan, “Learning a sparse transformer network for effective image deraining,” in *Proceedings of the IEEE/CVF Conference on Computer Vision and Pattern Recognition (CVPR)*, June 2023, pp. 5896–5905.
- [56] L. Kong, J. Dong, J. Ge, M. Li, and J. Pan, “Efficient frequency domain-based transformers for high-quality image deblurring,” in *Proceedings of the IEEE/CVF Conference on Computer Vision and Pattern Recognition*, 2023, pp. 5886–5895.
- [57] J. Xiao, X. Fu, A. Liu, F. Wu, and Z.-J. Zha, “Image de-raining transformer,” *IEEE Transactions on Pattern Analysis and Machine Intelligence*, vol. 45, no. 11, pp. 12 978–12 995, 2023.
- [58] T. Brooks, B. Mildenhall, T. Xue, J. Chen, D. Sharlet, and J. T. Barron, “Unprocessing images for learned raw denoising,” 2018.
- [59] C. Chen, C. Qifeng, X. Jia, and K. Vladlen, “Learning to see in the dark,” in *The IEEE Conference on Computer Vision and Pattern Recognition (CVPR)*, 2018.
- [60] O. Kupyn, T. Martyniuk, J. Wu, and Z. Wang, “Deblurgan-v2: Deblurring (orders-of-magnitude) faster and better,” *2019 IEEE/CVF International Conference on Computer Vision (ICCV)*, pp. 8877–8886, 2019.
- [61] X. Li, W. Wang, X. Hu, and J. Yang, “Selective kernel networks,” in *Proceedings of the IEEE/CVF conference on computer vision and pattern recognition*, 2019, pp. 510–519.
- [62] H. Zhang, V. A. Sindagi, and V. M. Patel, “Image de-raining using a conditional generative adversarial network,” *IEEE Transactions on Circuits and Systems for Video Technology*, vol. 30, pp. 3943–3956, 2017.
- [63] K. Jiang, Z. Wang, P. Yi, C. Chen, B. Huang, Y. Luo, J. Ma, and J. Jiang, “Multi-scale progressive fusion network for single image deraining,” *CVPR*, 2020.
- [64] W. Yang, R. T. Tan, J. Feng, J. Liu, Z. Guo, and S. Yan, “Deep joint rain detection and removal from a single image,” *2017 IEEE Conference on Computer Vision and Pattern Recognition (CVPR)*, pp. 1685–1694, 2016.
- [65] X. Fu, J. Huang, X. Ding, Y. Liao, and J. W. Paisley, “Clearing the skies: A deep network architecture for single-image rain removal,” *IEEE Transactions on Image Processing*, vol. 26, pp. 2944–2956, 2016.
- [66] W. Wei, D. Meng, Q. Zhao, and Z. Xu, “Semi-supervised cnn for single image rain removal,” *ArXiv*, vol. abs/1807.11078, 2018.
- [67] H. Zhang and V. M. Patel, “Density-aware single image de-raining using a multi-stream dense network,” *2018 IEEE/CVF Conference on Computer Vision and Pattern Recognition*, pp. 695–704, 2018.
- [68] R. Yasarla and V. M. Patel, “Uncertainty guided multi-scale residual learning—using a cycle spinning cnn for single image de-raining,” *2019 IEEE/CVF Conference on Computer Vision and Pattern Recognition (CVPR)*, pp. 8397–8406, 2019.
- [69] K. Purohit, M. Suin, A. N. Rajagopalan, and V. N. Boddeti, “Spatially-adaptive image restoration using distortion-guided networks,” *CoRR*, vol. abs/2108.08617, 2021.
- [70] X. Feng, H. Ji, W. Pei, J. Li, G. Lu, and D. Zhang, “U2-former: Nested u-shaped transformer for image restoration via multi-view contrastive learning,” *IEEE Transactions on Circuits and Systems for Video Technology*, pp. 1–1, 2023.
- [71] Z. Hao, S. Gai, and P. Li, “Multi-scale self-calibrated dual-attention lightweight residual dense deraining network based on monogenic wavelets,” *IEEE Transactions on Circuits and Systems for Video Technology*, vol. 33, no. 6, pp. 2642–2655, 2023.
- [72] W. Wu, Y. Liu, and Z. Li, “Subband differentiated learning network for rain streak removal,” *IEEE Transactions on Circuits and Systems for Video Technology*, vol. 33, no. 9, pp. 4675–4688, 2023.
- [73] D. Kingma and J. Ba, “Adam: A method for stochastic optimization,” *Computer Science*, 2014.
- [74] I. Loshchilov and F. Hutter, “Sgdr: Stochastic gradient descent with warm restarts,” 2016.
- [75] S. Nah, T. H. Kim, and K. M. Lee, “Deep multi-scale convolutional neural network for dynamic scene deblurring,” *2017 IEEE Conference on Computer Vision and Pattern Recognition (CVPR)*, pp. 257–265, 2016.
- [76] Z. Shen, W. Wang, X. Lu, J. Shen, H. Ling, T. Xu, and L. Shao, “Human-aware motion deblurring,” *2019 IEEE/CVF International Conference on Computer Vision (ICCV)*, pp. 5571–5580, 2019.
- [77] Y. Zhang, Q. Li, M. Qi, D. Liu, J. Kong, and J. Wang, “Multi-scale frequency separation network for image deblurring,” *IEEE Transactions on Circuits and Systems for Video Technology*, vol. 33, no. 10, pp. 5525–5537, 2023.
- [78] O. Kupyn, V. Budzan, M. Mykhailych, D. Mishkin, and J. Matas, “Deblurgan: Blind motion deblurring using conditional adversarial networks,” *2018 IEEE/CVF Conference on Computer Vision and Pattern Recognition*, pp. 8183–8192, 2017.
- [79] H. Gao, X. Tao, X. Shen, and J. Jia, “Dynamic scene deblurring with parameter selective sharing and nested skip connections,” *2019 IEEE/CVF Conference on Computer Vision and Pattern Recognition (CVPR)*, pp. 3843–3851, 2019.
- [80] K. Zhang, W. Luo, Y. Zhong, L. Ma, B. Stenger, W. Liu, and H. Li, “Deblurring by realistic blurring,” *2020 IEEE/CVF Conference on Computer Vision and Pattern Recognition (CVPR)*, pp. 2734–2743, 2020.
- [81] D. Park, D. U. Kang, J. Kim, and S. Y. Chun, “Multi-temporal recurrent neural networks for progressive non-uniform single image deblurring with incremental temporal training,” in *European Conference on Computer Vision*, 2019.
- [82] M. Suin, K. Purohit, and A. N. Rajagopalan, “Spatially-attentive patch-hierarchical network for adaptive motion deblurring,” *2020 IEEE/CVF Conference on Computer Vision and Pattern Recognition (CVPR)*, pp. 3603–3612, 2020.
- [83] S. J. Cho, S. W. Ji, J. P. Hong, S. W. Jung, and S. J. Ko, “Rethinking coarse-to-fine approach in single image deblurring,” in *ICCV*, 2021.